RSC Advances

PAPER

View Article Online
View Journal | View Issue

Cite this: *RSC Adv.*, 2021, **11**, 30911

Improved performance of a samarium-doped ceria interlayer of intermediate temperature solid oxide electrolysis cells by doping the transition metal oxide Fe_2O_3

Yanmei Qu, Ji Yu, Ning Tian* and Hai Shen

The ionic conductivity of the interlayer in the intermediate temperature solid oxide electrolysis cell (IT-SOEC) affects the polarization resistance of the oxygen electrode. Improving the ionic conductivity of the interlayer can improve the performance of the oxygen electrode. In this work, the ionic conductivity of a samarium-doped ceria (SDC) interlayer is improved by doping the transition metal oxide Fe_2O_3. The experimental results show that the oxygen electrode polarization resistance of the symmetrical cell based on the SDC-Fe_2O_3 interlayer is 0.09 Ω cm^{-2} at 800 °C and under the open circuit voltage, which is obviously lower than that of the symmetrical cell based on an SDC interlayer (0.22 Ω cm^{-2}). Besides, the electrolysis current of the SOEC based on the SDC-Fe_2O_3 interlayer is 0.5 A cm^{-2} at 800 °C and 1.5 V, which is higher than that of the SOEC based on the SDC interlayer (0.3 A cm^{-2}). The above results show that improving the ionic conductivity of the SDC interlayer in the SOEC by doping Fe_2O_3 can reduce the polarization resistance of the oxygen electrode and enhance the performance of the SOEC. Thus, this work provides an effective way for improving the performance of the SDC interlayer in the IT-SOEC.

Received 6th June 2021
Accepted 9th September 2021

DOI: 10.1039/d1ra04361g

rsc.li/rsc-advances

1. Introduction

Due to the depletion of traditional fossil energy and the serious environmental pollution caused by the use of traditional fossil energy, human beings attach great importance to the development of green and efficient energy.[1–4] Hydrogen energy has the advantages of being green, environmentally protective and highly efficient, and is expected to become the mainstream energy for the development of human society in the future.[5–7] Therefore, countries all over the world devote great efforts to the development of advanced hydrogen production technology.

The solid oxide electrolysis cell (SOEC) is considered as an excellent and ideal hydrogen production technology because of its solid-state structure, no pollutant emission and high electrode reactivity.[8–12] Currently, yttria-stabilized zirconia (YSZ) with low electron conductivity is the dominant electrolyte material for the intermediate temperature SOEC (IT-SOEC). In the process of preparation and operation of IT-SOECs, the Sr element in Sr-containing oxygen electrode materials (*e.g.*, $Ba_{1-x}Sr_xCo_yFe_{1-y}O_{3-\delta}$, $La_{1-x}Sr_xFeO_{3-\delta}$, $La_{1-x}Sr_xCoO_{3-\delta}$, $La_{1-x}Sr_xCo_{1-y}Fe_yO_{3-\delta}$, *etc.*) is easy to diffuse and react with the Zr element in YSZ electrolyte to form the $SrZrO_3$ insulating phase. This hinders the transportation of oxygen ions from the electrolyte to the oxygen electrode, and thereby increases the polarization resistance of the oxygen electrode and affects the electrolytic performance of the IT-SOEC. To prevent the solid-state reactions, a doped ceria interlayer is added between the YSZ electrolyte and Sr-containing oxygen electrode to inhibit Sr diffusion and avoid the generation of the $SrZrO_3$ insulating phase, so as to improve the performance of the oxygen electrode.[13–15] A lot of work has been done to improve the interlayer performance of IT-SOECs. For example, Kazuki Shimura *et al.* prepared a dense samarium-doped ceria (SDC) interlayer with uniform thickness by optimizing the preparation process, which made the oxygen ions be uniformly transported to the oxygen electrode, expanded the effective reaction area and improved the performance of the SOEC.[13] Sun Jae Kim *et al.* studied the effect of the density of a Gd-doped ceria (GDC) interlayer on the polarization resistance stability of the oxygen electrode. Three kinds of GDC interlayers were prepared by sputtering and firing at 1300 °C for 5 h, sputtering and firing at 1100 °C for 2 h, and screen printing and firing at 1300 °C for 5 h, respectively. The oxygen electrode polarization resistance of a SOEC based on a GDC interlayer deposited by sputtering and annealed at 1300 °C was the most stable because the GDC interlayer was compact and had no pinholes, which was beneficial to hinder the diffusion of the Sr element.[14] Hyun Jong Choi *et al.* reported that the transition metal oxide CuO additive was used to reduce the sintering temperature of the GDC interlayer,

College of Physics Science and Technology, Shenyang Normal University, Shenyang 110034, China. E-mail: yuji4268@synu.edu.cn; tiann08@synu.edu.cn

and realize co-sintering of the GDC interlayer with the LSCF air electrode.[15] By reducing the sintering temperature of the GDC interlayer, the solid-state reaction between the interlayer and YSZ electrolyte can be prevented. Solid state reaction would occur between the YSZ electrolyte and the GDC interlayer during high-temperature sintering. It forms a solid solution with lower conductivity as compared to that of GDC or YSZ. This is not conducive to the transport of oxygen ions. So too high a sintering temperature of the interlayer should be avoided. By adding CuO in the GDC interlayer, the sintering temperature of the interlayer is reduced, so as to prevent the solid-state reaction between the interlayer and YSZ electrolyte.[16–19] In addition, co-sintering can reduce the cost of the manufacturing process by reducing the necessary heat-treatment temperature, which is conducive to the commercialization of SOECs. It can be seen that improving the interlayer performance can enhance the performance of the oxygen electrode and the SOEC.

Since the interlayer can not only inhibit the diffusion of Sr but also act as a bridge to transport oxygen ions from the electrolyte to the oxygen electrode, the interlayer performance can be improved by increasing its density and oxygen ion conduction. It is reported that the transition metal oxide Fe_2O_3 can play the role of a sintering aid and grain boundary cleaning agent for the doped ceria electrolyte,[20–24] so doping Fe_2O_3 can improve the density and oxygen ion conduction of the doped ceria interlayer. Based on this, this work will study the effect of the transition metal oxide Fe_2O_3 on the performance of a samarium-doped ceria (SDC) interlayer of IT-SOECs. Generally, the sintering temperature of the SDC interlayer of IT-SOECs is 1250 °C,[5,25,26] and a higher sintering temperature will lead to the solid state reaction between the SDC interlayer and YSZ electrolyte. Besides, the optimum content of Fe_2O_3 in the SDC-Fe_2O_3 electrolyte is 0.25 mol%.[23,24] So the effect of 0.25 mol% Fe_2O_3 additive on the properties of the SDC interlayer sintered at 1250 °C will be studied in this work.

2. Experimental

2.1 Preparation of the samples

Both SDC and SDC-Fe_2O_3 electrolyte materials were prepared by glycine-nitrate method.[23] YSZ ($(Y_2O_3)_{0.08}(ZrO_2)_{0.92}$) electrolyte material was purchased from the Ningbo SOFCMAN Energy Technology Co., Ltd. $(La_{0.6}Sr_{0.4})_{0.95}Co_{0.2}Fe_{0.8}O_{3-\delta}$ (LSCF) oxygen electrode material was purchased from the Nexceris, LLC, Fuelcellmaterials, Lewis Center, OH, USA. NiO hydrogen electrode material was prepared by glycine-nitrate method. SDC and SDC-Fe_2O_3 electrolyte sheets were prepared by pressing SDC and SDC-Fe_2O_3 powders into green sheets with a diameter of 16 mm at 10 MPa, and sintering at 1250 °C for 4 h. YSZ electrolyte sheets were made by pressing YSZ powder into green sheets with diameter of 16 mm at 10 MPa and sintering at 1400 °C for 4 h. NiO–YSZ support was prepared by pressing NiO powder, YSZ powder and starch with a mass ratio of 5 : 5 : 2 into green sheets with diameter of 16 mm at 1 MPa and sintering at 1000 °C for 4 h. LSCF–SDC/SDC/YSZ/SDC/LSCF–SDC or LSCF–SDC/SDC-Fe_2O_3/YSZ/SDC-Fe_2O_3/LSCF–SDC structured symmetrical cell was obtained by painting SDC or SDC-Fe_2O_3 interlayer on both sides of YSZ electrolyte by screen printing and sintering at 1250 °C for 4 h, and then LSCF–SDC oxygen electrode material (the mass ratio of LSCF to SDC was 7 : 3) was coated on the interlayers by screen printing and sintering at 1000 °C for 4 h. NiO–YSZ/YSZ/SDC/LSCF–SDC or NiO–YSZ/YSZ/SDC-Fe_2O_3/LSCF–SDC structured SOEC was prepared as follows: YSZ electrolyte layer was coated on NiO–YSZ support by screen printing and sintered at 1400 °C for 4 h. Then SDC or SDC-Fe_2O_3 interlayer was coated on YSZ electrolyte layer by screen printing and sintered at 1250 °C for 4 h. Next, LSCF–SDC oxygen electrode material was screen printed on the surface of the interlayer and sintered at 1000 °C for 4 h. Silver paste was used to seal the SOEC, and silver paste was used as the collector of oxygen electrode and hydrogen electrode, and silver wire was used as the conductor of the SOEC. Note that the effective oxygen electrode area of the above symmetric cells and SOECs was 0.4 × 0.4 cm^2.

2.2 Measurement of the samples

The crystal structure of SDC and SDC-Fe_2O_3 powder samples was characterized by a Japan Rigaku-D-Max Ra X-ray diffractometer (XRD). The surface morphologies of SDC and SDC-Fe_2O_3 electrolyte sheets, the surface and cross section morphologies of SDC and SDC-Fe_2O_3 interlayer were characterized by scanning electron microscope (SEM, FEI Quanta 250 FEG). The electrochemical impedance spectra of electrolyte sheets, symmetrical cells, and SOECs were characterized by an electrochemical workstation (CHI 760E, Shanghai Chenhua Instrument Corporation, China) with the frequency range of 0.1 Hz to 1 MHz and a signal amplitude of 50 mV. The current density–voltage characteristic curve of the SOEC was measured by a linear voltage sweep at a scanning rate of 9 mV s^{-1}.

3. Results and discussion

Fig. 1(a) shows the XRD patterns of SDC and SDC-Fe_2O_3 powder samples calcined at 1250 °C for 4 h. It can be seen that both samples have a cubic fluorite phase of CeO_2. No secondary phases (Fe_2O_3 or Fe-related impurities) are found in the XRD spectrum of SDC-Fe_2O_3. To study the effect of Fe_2O_3 on SDC lattice structure, the Rietveld refinement is performed on SDC and SDC-Fe_2O_3 samples. The results of the Rietveld refinement for SDC and SDC-Fe_2O_3 samples are shown in the Fig. 1(b) and (c), respectively. The lattice constant of SDC and SDC-Fe_2O_3 samples is 0.5442 nm and 0.5435 nm, respectively. It can be noted that the lattice constant of SDC-Fe_2O_3 is slightly lower than that of SDC. This decrease may be due to the substitution of Ce^{4+} ions ($r = 0.097$ nm) by smaller Fe^{3+} ions ($r = 0.078$ nm) in the cubic lattice of CeO_2 structure.[23]

Scanning electron micrograph (SEM) of SDC and SDC-Fe_2O_3 electrolyte sheets sintered at 1250 °C for 4 h is shown in the Fig. 2(a) and (b), respectively. It can be found that the SDC-Fe_2O_3 electrolyte sheet is more dense, while the SDC electrolyte sheet has many pores. To study the density of the two electrolytes, the density of the two electrolytes is measured by Archimedes' method. The relative density of the two electrolyte sheets is 90% and 97% respectively, which indicates that the

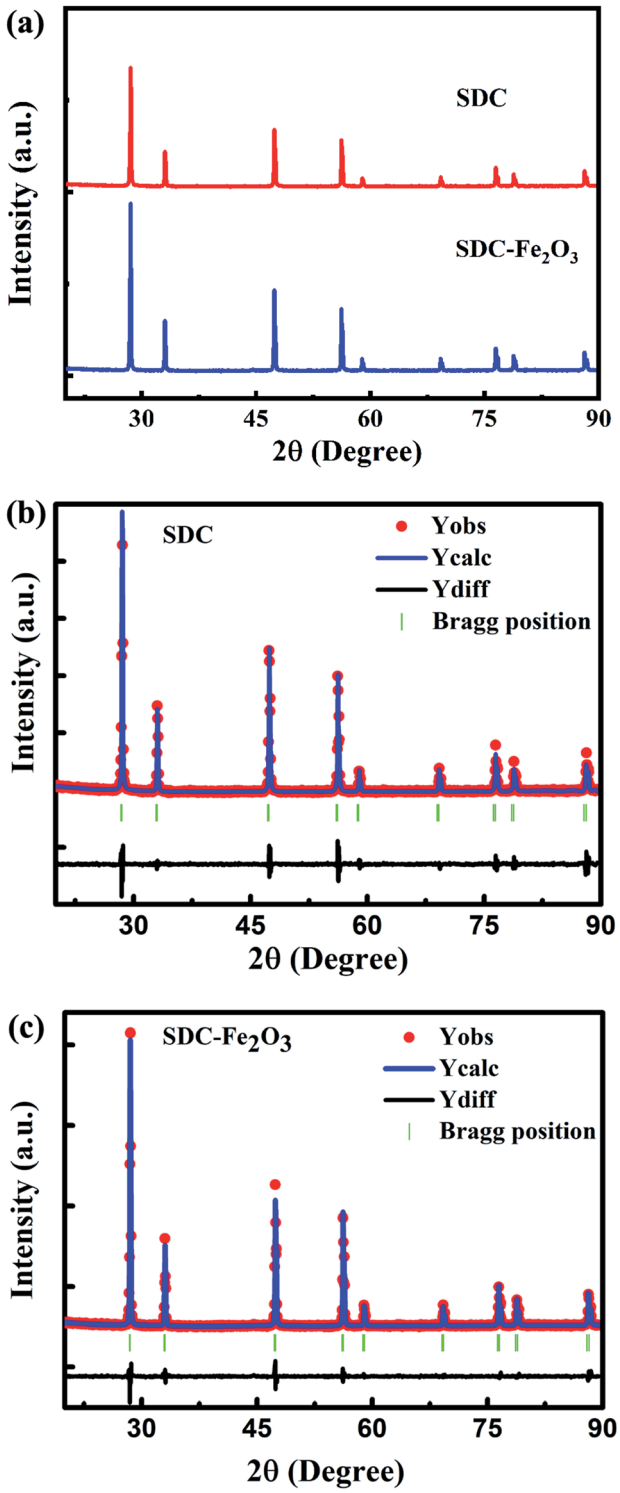

Fig. 1 (a) XRD patterns of SDC and SDC-Fe_2O_3 powder samples calcined at 1250 °C for 4 h. XRD Rietveld refinement result of SDC sample (b) and SDC-Fe_2O_3 sample (c). Where, the value of R_{wp} for SDC and SDC-Fe_2O_3 samples is 7.3% and 5.2%, respectively.

dense SDC electrolyte sheets can be obtained by doping Fe_2O_3. It also illustrates that the compactness of SDC interlayer of SOEC sintered at 1250 °C for 4 h can be enhanced by doping Fe_2O_3.

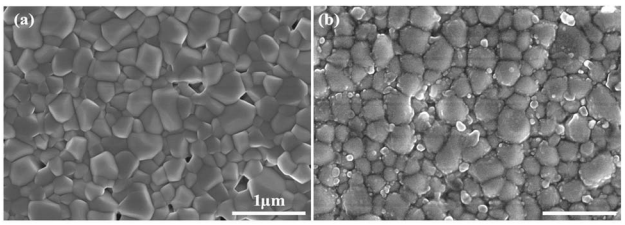

Fig. 2 Scanning electron micrograph (SEM) of SDC (a) and SDC-Fe_2O_3 (b) electrolyte sheets sintered at 1250 °C for 4 h.

The temperature dependences of the grain interior conductivity, the grain boundary conductivity and total conductivity of SDC and SDC-Fe_2O_3 electrolyte sheets are shown in Fig. 3. From the Fig. 3(a), it can be noted that the grain interior conductivity of the SDC-Fe_2O_3 electrolyte sheet is similar with that of the SDC electrolyte sheet at 300–500 °C, which suggests that adding Fe_2O_3 has little impact on grain interior conductivity of SDC. This means that little Fe element is incorporated within the bulk structure of SDC, which is consistent with the XRD results. From the Fig. 3(b), it can be found that the grain boundary conductivity of SDC-Fe_2O_3 electrolyte sheet is obviously higher than that of SDC electrolyte sheet. It suggests that adding Fe_2O_3 can significantly enhance the SDC grain boundary conductivity. The possible reason is that Fe_2O_3 plays a role in reducing SDC grain boundary blocking effect caused by the siliceous layers and space charge effects, thus improving the oxygen ion conduction of SDC grain boundary.[20–22] From the Fig. 3(c), it can be seen that the total conductivity of SDC-Fe_2O_3 is higher than that of SDC. It indicates that the total conduction of SDC is dominated by grain boundary conduction. Therefore, it can be concluded that the oxygen ion conduction of SDC interlayer can be improved by doping Fe_2O_3.

Fig. 4(a) and (b) are the SEMs of SDC and SDC-Fe_2O_3 interlayer, respectively. It can be seen that both SDC and SDC-Fe_2O_3 interlayers are relatively dense, which can block Sr diffusion, and provide more transport channels for oxygen ions from YSZ to the oxygen electrode.[13] Fig. 4(c) and (d) are the cross-section SEMs of LSCF–SDC/SDC/YSZ and LSCF–SDC/SDC-Fe_2O_3/YSZ structures, respectively. It can be found that the interlayers are closely combined with the YSZ layers and the oxygen electrode layers. It ensures the stability of the SOEC structure.

Fig. 5(a) shows the AC impedance spectra of symmetrical cells based on SDC and SDC-Fe_2O_3 interlayer at 800 °C and under the open circuit voltage (OCV). To directly compare the polarization impedance of the two symmetrical cells, the ohmic impedance is subtracted from the impedance spectra. It can be seen that the oxygen electrode polarization resistance (R_p) of the symmetrical cell based on SDC-Fe_2O_3 interlayer is obviously lower than that of the symmetrical cell based on SDC interlayer. This is because doping Fe_2O_3 in SDC improves its oxygen ion conduction. Oxygen ions migrated from the YSZ electrolyte can move faster to the oxygen electrode to participate in the electrochemical reaction, and thereby reduces the polarization resistance of the oxygen electrode. This means that the polarization resistance of the SOEC oxygen electrode can be reduced

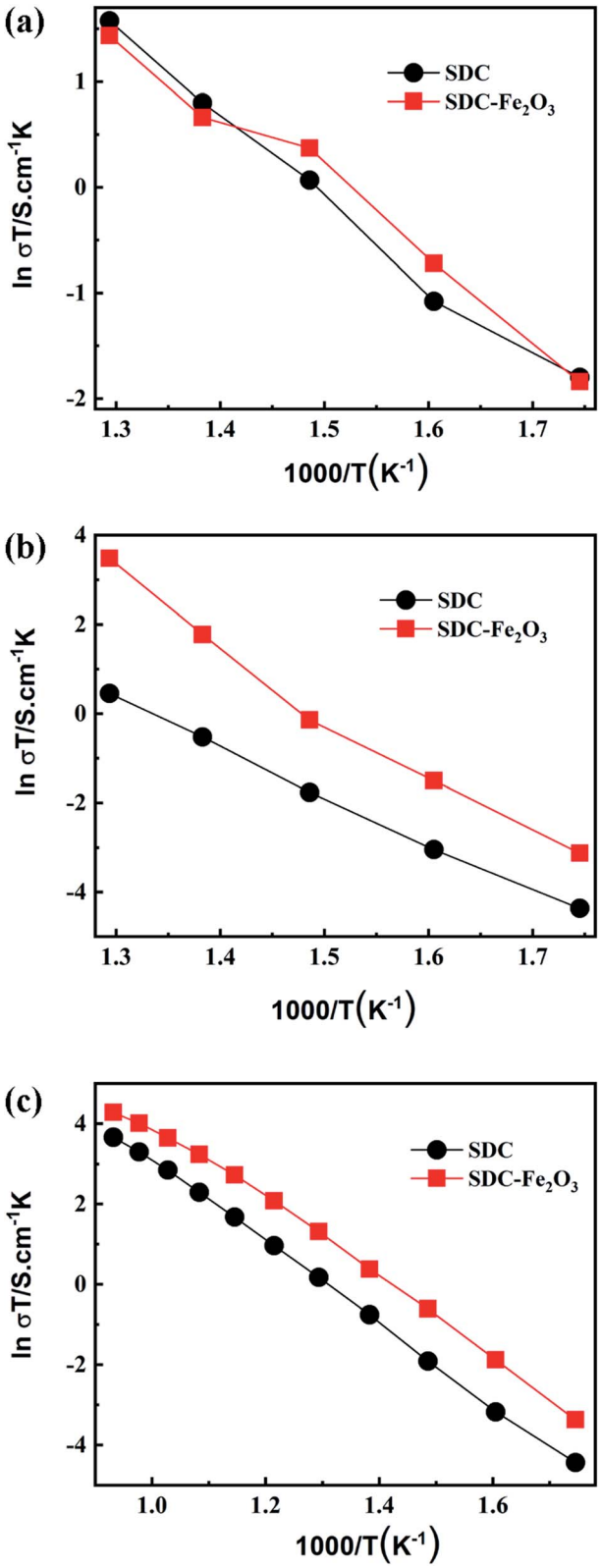

Fig. 3 The temperature dependences of the grain interior conductivity (a), the grain boundary conductivity (b) and the total conductivity (c) of SDC and SDC-Fe_2O_3 electrolyte sheets.

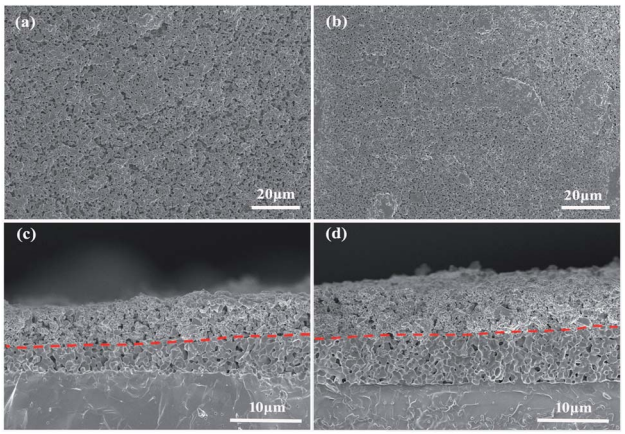

Fig. 4 Interlayer surface morphologies of (a) SDC and (b) SDC-Fe_2O_3, and cross-sectional morphologies of (c) LSCF–SDC/SDC/YSZ and (d) LSCF–SDC/SDC-Fe_2O_3/YSZ structures.

by improving the ionic conductivity of the interlayer. Equivalent circuit of $R_o(R_H/CPE_H)(R_L/CPE_L)$ is carried out to fit the spectra, where R_o is the ohmic resistance, CPE is the constant phase element, the subscripts H and L correspond to the high and low-frequency arc respectively, and $R_p = R_H + R_L$. The fitting values of R_H, R_L and R_p of the symmetrical cells are listed in Table 1. The R_p value of the LSCF oxygen electrode in our case is 0.09 Ω cm^2. Zehua Pan *et al.* reported the high performance LSCF oxygen electrode with the R_p of 0.042 Ω cm^2.[27] Bo Wei *et al.* reported the remarkable performance LSCF oxygen electrode with the R_p of 0.06 Ω cm^2.[28] Evidently, the performance of the LSCF oxygen electrode in our case can be comparable to that of the reported LSCF oxygen electrode with remarkable performance.

Stability is an important parameter to evaluate the SOEC performance. The stability of the symmetrical cells based on SDC and SDC-Fe_2O_3 interlayer at 800 °C is shown in Fig. 5(b), in which the test time is 30 h and the anodic current is 0.8 A cm^{-2}. During the test, AC impedance measurements of the symmetrical cells are carried out per 5 h under OCV conditions with interrupting the electrolysis test. It can be seen that the oxygen electrode polarization resistance decay rate (0.16 mΩ cm^2 h^{-1}) of the symmetrical cell based on the SDC-Fe_2O_3 interlayer is lower than that (0.78 mΩ cm^2 h^{-1}) of the symmetrical cell based on the SDC interlayer, which indicates that enhancing the ionic conductivity of the interlayer is conducive to improving the stability of the oxygen electrode.

Fig. 6(a) shows the current density–voltage curve of the SOECs based on SDC and SDC-Fe_2O_3 interlayer at 800 °C. It can be noted that the electrolysis current of the SOEC based on SDC-Fe_2O_3 interlayer is higher than that of the SOEC based on SDC interlayer. It indicates that improving the oxygen ion conduction of the interlayer will make oxygen ions move faster to participate in the oxygen evolution reaction of the oxygen electrode, which reduces the polarization resistance of the oxygen electrode and increases the electrolysis current of the SOEC. At 1.5 V, the electrolysis current of the SOEC based on SDC-Fe_2O_3 interlayer can be 0.5 A cm^{-2}, which is obviously higher than that of the SOEC based on SDC interlayer (0.3 A cm^{-2}). The

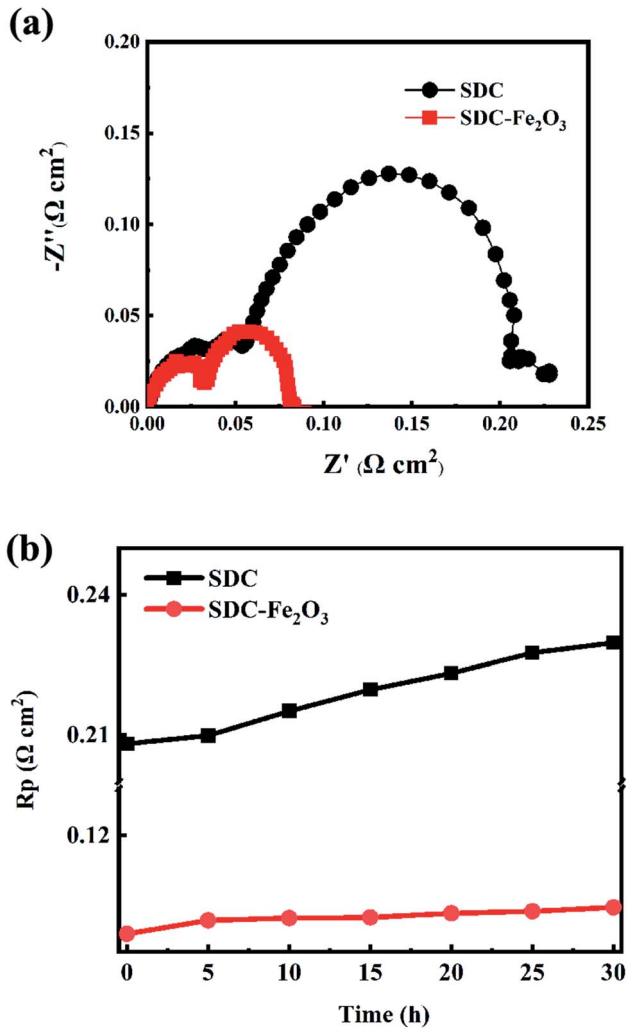

Fig. 5 (a) AC impedance spectra of symmetrical cells based on SDC and SDC-Fe_2O_3 interlayer at 800 °C and under the open circuit voltage (OCV). (b) The stability of the symmetrical cells based on SDC and SDC-Fe_2O_3 interlayer at 800 °C.

Table 1 The fitting values of R_H, R_L and R_p of the symmetrical cells based on SDC and SDC-Fe_2O_3 interlayer obtained by an equivalent circuit fitting of the impedance spectra. Note that the unit of R is Ω cm^2

	R_H	R_L	R_p
SDC	0.08	0.14	0.22
SDC-Fe_2O_3	0.04	0.05	0.09

comparison of the electrolysis current density for the SOECs is provided in Table 2 to evaluate the performance of the SOEC in this work. Clearly, the performance of the SOEC based on SDC-Fe_2O_3 interlayer in our case can be comparable to that of the reported SOECs with remarkable performance. The hydrogen production rate of the SOECs can be calculated from the measured current as follows:[29]

$$\Delta N_{H_2} = \frac{-I}{2F}$$

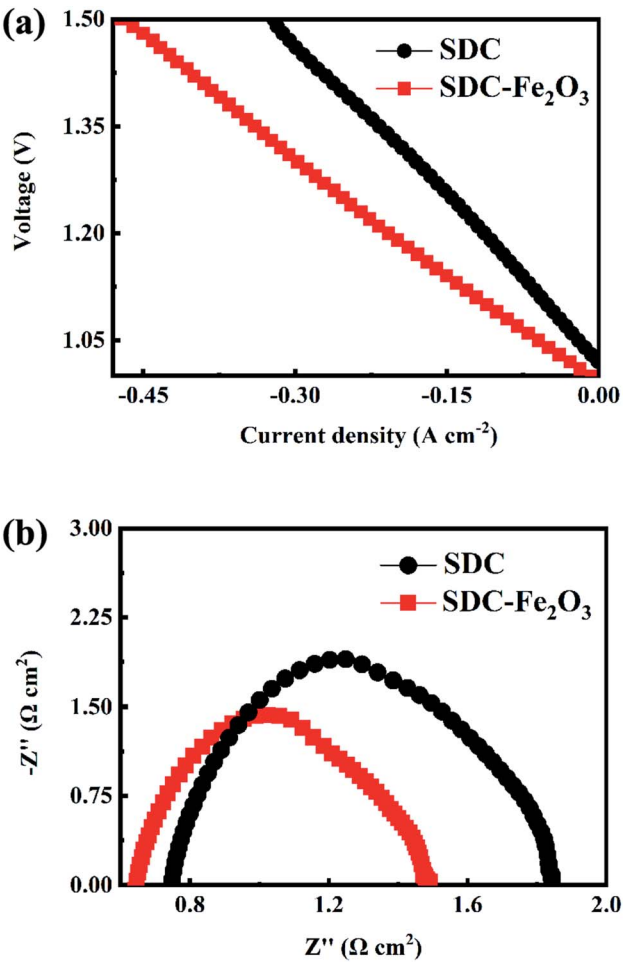

Fig. 6 (a) Current density–voltage curve of the SOECs based on SDC and SDC-Fe_2O_3 interlayer at 800 °C. (b) Impedance spectra of the two SOECs based on SDC and SDC-Fe_2O_3 interlayer at 800 °C and under OCV.

where ΔN_{H2} is the molar rate of hydrogen production; I is the electrical current and F is Faraday's constant. At 800 °C, the calculated hydrogen production rate of the SOECs based on SDC and SDC-Fe_2O_3 interlayer at 1.5 V is 132 and 195 ml cm^{-2} h^{-1}, respectively.

Fig. 6(b) shows the impedance spectra of the two SOECs at 800 °C and under OCV. Equivalent circuit of $R_o(R_p/CPE_p)$ is carried out to fit the spectra, and the ohmic resistance and polarization resistance of the two SOECs are listed in Table 3. It can be seen that the ohmic resistance of the SOEC based on SDC-Fe_2O_3 interlayer is lower than that of the SOEC based on SDC interlayer. The ohmic resistance of a single cell is the sum of electrodes resistance, electrolyte resistance, interlayer resistance and contact resistance. The difference of ohmic resistance between the two SOECs may be caused by the ionic conductivity of the interlayers. The polarization resistance of the SOEC based on SDC-Fe_2O_3 interlayer is significantly lower than that of the SOEC based on SDC interlayer. Because both of them have the hydrogen electrode prepared under the same conditions, the difference of polarization resistance is due to the difference of

Table 2 Comparison of the electrolysis current density for the SOECs at 1.5 V and 800 °C

SOEC	Electrolysis current density (A cm^{-2})	Feed gas	Ref.
PSTF|YSZ|LSM–YSZ	0.3	60% H_2O/Ar	30
NiO–YSZ/YSZ/LSF–YSZ	0.8	50% H_2O + 25% H_2 + 25% N_2	31
YSZ–NiO|GDC|SSZ|LSC	0.5	60% H_2O/H_2	32
Ni–YSZ|YSZ|GDC|LSCF	1.5	50% H_2O + 50% H_2	33
Ni–YSZ|YSZ|GDC|GBCO–GDC	0.6	NA	34
Ni–YSZ|YSZ|SDC-Fe_2O_3|LSCF–SDC	0.5	40% H_2O/N_2	This work

Table 3 The fitting values of R_o and R_p of the SOECs based on SDC and SDC-Fe_2O_3 interlayer. Note that the unit of R is Ω cm^2

	R_o	R_p
SDC	0.74	0.97
SDC-Fe_2O_3	0.64	0.74

oxygen electrode. It is proved again that improving the oxygen ion conductivity of SOEC interlayer can reduce the polarization resistance of the oxygen electrode.

4. Conclusions

In this work, the ionic conductivity of SDC interlayer of the SOEC is improved by doping the transition metal oxide Fe_2O_3, thus the polarization resistance of oxygen electrode is reduced and the performance of the SOEC is improved. The experimental results show that the oxygen electrode polarization resistance of the symmetrical cell based on SDC-Fe_2O_3 interlayer is obviously lower than that of the symmetrical cell based on SDC interlayer, and the electrolysis current of the SOEC based on SDC-Fe_2O_3 interlayer is higher than that of the SOEC based on SDC interlayer. The above results indicate that doping Fe_2O_3 with SDC interlayer is an effective method for improving the SDC interlayer performance of IT-SOEC.

Conflicts of interest

There are no conflicts to declare.

Acknowledgements

This study was financed by Natural Science Foundation of Liaoning Province (2019JH3/30100036, 2019-ZD-0480).

References

1 S. Hiroyuki, Y. Toshiaki, K. Haruo, S. Hirofumi, Y. Yuki, N. Katsuhiro and F. Yoshinobu, Nanocomposite electrodes for high current density over 3 A cm^{-2} in solid oxide electrolysis cells, *Nat. Commun.*, 2019, **10**, 5432, DOI: 10.1038/s41467-019-13426-5.

2 J. Kim, A. Jun, O. Gwon, S. Yoo, M. Liu, J. Shin, T. H. Lim and G. Kim, Hybrid-solid oxide electrolysis cell: A new strategy for efficient hydrogen production, *Nano Energy*, 2018, **44**, 121–126, DOI: 10.1016/j.nanoen.2017.11.074.

3 D. Nikolay, J. Lyagaeva, G. Vdovin and D. Medvedev, Multifactor performance analysis of reversible solid oxide cells based on proton-conducting electrolytes, *Appl. Energy*, 2019, **237**, 924–934, DOI: 10.1016/j.apenergy.2019.01.054.

4 L. Bi, S. P. Shaf and E. Traversa, Y-doped $BaZrO_3$ as a chemically stable electrolyte for proton-conducting solid oxide electrolysis cells (SOECs), *J. Mater. Chem. A*, 2015, **3**, 5815–5819, DOI: 10.1039/c4ta07202b.

5 Y. Tan, N. Q. Duan, A. Wang, D. Yan, B. Chi, N. Wang, J. Pu and J. Li, Performance enhancement of solution impregnated nanostructured $La_{0.8}Sr_{0.2}Co_{0.8}Ni_{0.2}O_{3-d}$ oxygen electrode for intermediate temperature solid oxide electrolysis cells, *J. Power Sources*, 2016, **305**, 168–174, DOI: 10.1016/j.jpowsour.2015.11.094.

6 M. D. Liang, B. Yu, M. F. Wen, J. Chen, J. M. Xu and Y. C. Zhai, Preparation of LSM–YSZ composite powder for anode of solid oxide electrolysis cell and its activation mechanism, *J. Power Sources*, 2009, **190**, 341–345, DOI: 10.1016/j.jpowsour.2008.12.132.

7 W. Jiang, B. Wei, Z. Lü, Z. H. Wang, L. Zhu and Y. Q. Li, Performance and stability of co-synthesized $Sm_{0.5}Sr_{0.5}CoO_3$-$Ce_{0.8}Sm_{0.2}O_{1.9}$ composite oxygen electrode for solid oxide electrolysis cells, *Int. J. Hydrogen Energy*, 2015, **40**, 561–567, DOI: 10.1016/j.ijhydene.2014.10.128.

8 L. B. Lei, Z. T. Tao, X. M. Wang, J. P. Lemmon and F. L. Chen, Intermediate-temperature solid oxide electrolysis cells with thin proton-conducting electrolyte and robust air electrode, *J. Mater. Chem. A*, 2017, **5**, 2904–2910, DOI: 10.1039/C7TA05841A.

9 Y. F. Zheng, H. Yang, Z. H. Pan and C. Z. Zhang, A Ca and Fe Co-Doped Layered Perovskite as Stable Air Electrode in Solid Oxide Electrolyzer Cells under High-Current Electrolysis, *Electrochim. Acta*, 2017, **251**, 581–587, DOI: 10.1016/j.electacta.2017.08.172.

10 D. M. Huan, N. Shi, L. Zhang, W. Z. Tan, Y. Xie, W. H. Wang, C. R. Xia, R. R. Peng and Y. L. Lu, New, Efficient, and Reliable Air Electrode Material for Proton Conducting Reversible Solid Oxide Cells, *ACS Appl. Mater. Interfaces*, 2018, **10**, 1761–1770, DOI: 10.1021/acsami.7b16703.

11 H. Fan and M. F. Han, Improved performance and stability of Ag-infiltrated nanocomposite $La_{0.6}Sr_{0.4}Co_{0.2}Fe_{0.8}O3-\delta(Y_2O_3)_{0.08}(ZrO_2)_{0.92}$ oxygen electrode for H_2O/CO_2 co-electrolysis, *J. Power Sources*, 2016, **336**, 179–185, DOI: 10.1016/j.jpowsour.2016.10.046.

12 S. J. Yang, Y. B. Wen, J. C. Zhang, Y. Lu, X. F. Ye and Z. Y. Wen, Electrochemical performance and stability of cobalt-free $Ln_{1.2}Sr_{0.8}NiO_4$(Ln=La and Pr) air electrodes for proton-conducting reversible solid oxide cells, *J. Power Sources*, 2018, **267**, 269–277, DOI: 10.1016/j.electacta.2018.02.053.

13 K. Shimura, H. Nishino, K. Kakinuma, M. E. Brito and H. Uchida, Effect of samarium-doped ceria (SDC) interlayer on the performance of $La_{0.6}Sr_{0.4}Co_{0.2}Fe_{0.8}O_{3-\delta}$/SDC composite oxygen electrode for reversible solid oxide fuel cells, *Electrochim. Acta*, 2017, **225**, 114–120, DOI: 10.1016/j.electacta.2016.12.100.

14 S. J. Kim, S. W. Kim, Y. M. Park, K. J. Kim and G. M. Choi, Effect of Gd-doped ceria interlayer on the stability of solid oxide electrolysis cell, *Solid State Ionics*, 2016, **295**, 25–31, DOI: 10.1016/j.ssi.2016.07.007.

15 H. J. Choi, Y. H. Na, M. Kwak, T. W. Kim, D. W. Seo, S. K. Woo and S. D. Kim, Development of solid oxide cells by co-sintering of GDC diffusion barriers with LSCF air electrode, *Ceram. Int.*, 2017, **43**, 13653–13660, DOI: 10.1016/j.ceramint.2017.07.075.

16 V. Wilde, H. Störmer, J. Szász, F. Wankmüller, E. Ivers-Tiffée and D. Gerthsen, $Gd_{0.2}Ce_{0.8}O_2$ Diffusion Barrier Layer between $(La_{0.58}Sr_{0.4})(Co_{0.2}Fe_{0.8})O_{3-\delta}$Cathode and $Y_{0.16}Zr_{0.84}O_2$ Electrolyte for Solid Oxide Fuel Cells:Effect of Barrier Layer Sintering Temperature on Microstructure, *ACS Appl. Energy Mater.*, 2018, **1**, 6790–6800, DOI: 10.1021/acsaem.8b00847.

17 H. Xu, K. Cheng, M. Chen, L. Zhang, K. Brodersen and Y. Du, Interdiffusion between gadolinia doped ceria and yttria stabilized zirconia in solid oxide fuel cells: Experimental investigation and kinetic modeling, *J. Power Sources*, 2019, **441**, 227152, DOI: 10.1016/j.jpowsour.2019.22715.

18 A. Tsoga, A. Gupta, A. Naoumidis and P. Nikolopoulos, Gadolinia-doped ceria and yttria stabilized zirconia interfaces: regarding their application for SOFC technology, *Acta Mater.*, 2000, **48**, 4709–4714, DOI: 10.1016/S1359-6454(00)00261-5.

19 R. Kiebach, W. W. Zhang, W. Zhang, M. Chen, K. Norrman, H. J. Wang, J. R. Bowen, R. Barfod and P. V. Hendriksen, Stability of $La_{0.6}Sr_{0.4}Co_{0.2}Fe_{0.8}O_3/Ce_{0.9}Gd_{0.1}O_2$ cathodes during sintering and solid oxide fuel cell operation, *J. Power Sources*, 2015, **283**, 151–161, DOI: 10.1016/j.jpowsour.2015.02.064.

20 H. J. Avila-Paredes and S. Kim, The effect of segregated transition metal ions on the grain boundary resistivity of gadolinium doped ceria: Alteration of the space charge potential, *Solid State Ionics*, 2006, **177**, 3075–3080, DOI: 10.1016/j.ssi.2006.08.017.

21 T. S. Zhang, J. Ma, L. B. Kong, S. H. Chan, P. Hing and J. A. Kilner, Iron oxide as an effective sintering aid and a grain boundary scavenger for ceria-based electrolytes, *Solid State Ionics*, 2004, **167**, 203–207, DOI: 10.1016/j.ssi.2004.01.006.

22 T. S. Zhang, J. Ma, Y. J. Leng and Z. M. He, Sintering, microstructure and grain growth of Fe-doped $Ce_{0.9}Gd_{0.1}O_2$dceramics derived from oxalate coprecipitation, *J. Cryst. Growth*, 2005, **274**, 603–611, DOI: 10.1016/j.jcrysgro.2004.10.011.

23 D. Xu, X. M. Liu, S. F. Xu, D. T. Yan, L. Pei, C. J. Zhu, D. J. Wang and W. H. Su, Fabrication and performance of $Ce_{0.85}Sm_{0.15}O_{1.925}$–$Fe_2O_3$ electrolytes in IT-SOFCs, *Solid State Ionics*, 2011, **192**, 510–514, DOI: 10.1016/j.ssi.2010.03.026.

24 N. Tian, Y. F. Deng, G. N. Li and X. W. Zhang, Electrical properties of $Ce_{0.85}Sm_{0.15}O_{1.925}eFe_2O_3$ electrolytes for IT-SOFCs, *J. Alloys Compd.*, 2016, **655**, 215–219, DOI: 10.1016/j.jallcom.2015.09.162.

25 A. Flura, C. Nicollet, V. Vibhu, A. Rougier, J. M. Bassat and J. C. Grenier, Ceria doped with praseodymium instead of gadolinium as efficient interlayer for lanthanum nickelate SOFC oxygen electrode, *Electrochim. Acta*, 2017, **231**, 103–114, DOI: 10.1016/j.electacta.2017.02.019.

26 J. Yu, H. J. Men, Y. M. Qu and N. Tian, Performance of Ni-Fe bimetal based cathode for intermediate temperature solid oxide electrolysis cell, *Solid State Ionics*, 2020, **346**, 115203, DOI: 10.1016/j.ssi.2019.115203.

27 Z. Pan, Q. Liu, R. Lyu, P. Li and S. H. Chan, Effect of $La_{0.6}Sr_{0.4}Co_{0.2}Fe_{0.8}O_{3-\delta}$ air electrode–electrolyte interface on the short-term stability under high-current electrolysis in solid oxide electrolyzer cells, *J. Power Sources*, 2018, **378**, 571–578, DOI: 10.1016/j.jpowsour.2018.01.002.

28 B. Wei, K. F. Chen, L. Zhao, Z. Lv and S. P. Jiang, Chromium deposition and poisoning at $La_{0.6}Sr_{0.4}Co_{0.2}Fe_{0.8}O_{3-\delta}$ oxygen electrodes of solid oxide electrolysis cells, *Phys. Chem. Chem. Phys.*, 2015, **17**, 1601–1609, DOI: 10.1039/C4CP05110F.

29 H. J. Men, N. Tian, Y. M. Qu, M. Wang, S. Zhao and J. Yu, Improved performance of a lanthanum strontium manganite-based oxygen electrode for an intermediate-temperature solid oxide electrolysis cell realized via ionic conduction enhancement, *Ceram. Int.*, 2019, **45**, 7945–7949, DOI: 10.1016/j.ceramint.2019.01.107.

30 L. J. Zhang, Z. H. Wang, Z. Q. Cao, L. Zhu, P. Z. Li, J. W. Li and Z. Lv, High activity oxide $Pr_{0.3}Sr_{0.7}Ti_{0.3}Fe_{0.7}O_{3-\delta}$ as cathode of SOEC for direct high-temperature steam electrolysis, *Int. J. Hydrogen Energy*, 2017, **42**, 12104–12110, DOI: 10.1016/j.ijhydene.2017.03.043.

31 H. Fan, Y. L. Zhang and M. F. Han, Infiltration of $La_{0.6}Sr_{0.4}FeO_{3-\delta}$ nanoparticles into YSZ scaffold for solid oxide fuel cell and solid oxide electrolysis cell, *J. Alloys Compd.*, 2017, **723**, 620–626, DOI: 10.1016/j.jallcom.2017.06.018.

32 Y. Y. Li, L. L. Yang, W. L. Li, Z. Y. Hou, C. X. Shi, G. J. Zhang, J. Zhou and S. R. Wang, A promising strontium and cobalt-free air electrode $Pr_{1-x}Ca_xFeO_{3-\delta}$ for solid oxide electrolysis cell, *Int. J. Hydrogen Energy*, 2021, **46**, 30230–30238, DOI: 10.1016/j.ijhydene.2021.06.185.

33 V. Vibhu, I. C. Vinke, R.-A. Eichel and L. G. J. de Haart, Cobalt substituted $Pr_2Ni_{1-x}CoxO_{4+\delta}$ (x = 0, 0.1, 0.2) oxygen electrodes: Impact on electrochemical performance and durability of solid oxide electrolysis cells, *J. Power Sources*, 2021, **482**, 228909, DOI: 10.1016/j.jpowsour.2020.228909.

34 S. M. Liu, W. Q. Zhang, Y. F. Li and B. Yu, $REBaCo_2O_{5+\delta}$(RE= Pr, Nd, and Gd) as promising oxygen electrodes for intermediate-temperature solid oxide electrolysis cells, *RSC Adv.*, 2017, **7**, 16332, DOI: 10.1039/c6ra28005f.